

A NOVEL MULTI-STEP FINITE-CONTROL-SET MODEL PREDICTIVE CONTROL APPROACH FOR PERMANENT MAGNET SYNCHRONOUS MOTORS

WEILIN YANG¹, ATABAYEV ARYSTAN¹, GUANYANG HU¹, DEZHI XU^{1,*}
WEIMING ZHANG¹ AND YAN XIA²

¹School of Internet of Things Engineering
Jiangnan University

No. 1800, Lihu Avenue, Wuxi 214122, P. R. China

*Corresponding author: xudezhi@jiangnan.edu.cn

²Department of Automation and Information Engineering
Sichuan University of Science and Engineering
No. 188, University Town, Yibin 643000, P. R. China

Received October 2020; revised February 2021

ABSTRACT. *In recent years, finite-control-set model predictive control (FCS-MPC) has been widely investigated in motor control, which is featured with fast dynamic response, great current control performance, and the ability of handling several kinds of constraints. In this paper, FCS-MPC of permanent magnet synchronous motors (PMSMs) is studied. The traditional one-step FCS-MPC approach is usually considered for the current control of PMSMs. However, large speed fluctuations and high current harmonics are observed. Although better control performance can be achieved by employing multi-step FCS-MPC strategies, the computational burden is usually heavy. Hence, a novel multi-step FCS-MPC strategy that is based on sector division is proposed in this paper to overcome the above issues. The multi-step cost function is transformed into a least squares problem through matrix transformation. In order to find the optimal control input (switch states), the following two steps are carried out. First, minimize the cost function via solving an optimization problem within the continuum space, which aims to locate the sector where the ideal switch states corresponding to the current time instant lie in; Second, the traversing method that determines the optimal switch states of the three-phase two-level inverter of a PMSM is adopted within the selected sector. The main advantage of the proposed approach is that multi-step predictions are achieved while the computation burden can be significantly reduced. Simulations reveal the effectiveness of the proposed method.*

Keywords: Finite-control-set model predictive control, Permanent magnet synchronous motor, Multi-step predictive control

1. **Introduction.** Model predictive control (MPC) has been widely used in process industries in the last three decades. Due to the rapid development of microprocessors, much attention has been paid to MPC in control of power converters and drives [1, 2, 3] since it is able to deal with multivariables together with constraints, and has satisfying dynamic responses [4, 5, 6]. However, the main problem MPC faces is to solve the computational burden, and power electronics need a quick control response to ensure the normal operation of the system [7, 8]. However, due to the fact that the computing power of modern microprocessors has increased dramatically, this makes it possible to implement more complex and intelligent control strategies. In general, the MPC controls the output of the

system by setting a cost function, and compares the error between the reference value and the predicted value by the cost function and selects the minimum value error to determine the control action. At each sampling instant, the MPC controller obtains a set of control sequences by minimizing the cost function, but only applies the first element of the set of sequences to the system and repeats this action at each sampling moment [9, 10]. MPC can be divided into continuous control set MPC (CCS-MPC) and finite control set MPC (FCS-MPC) according to the type of optimization problem [11, 12]. CCS-MPC calculates the continuous signal and then outputs the desired voltage to the power converter through the modulator [13]. FCS-MPC considers the discrete characteristics of the power converter, without an external modulator [14, 15].

Permanent magnet synchronous motors (PMSMs) have high efficiency, high power density and small size widely. They have been widely used in various fields, such as robots, elevators, and cars [16, 17, 18]. The prevailing high-performance control methods for PMSM are field oriented control (FOC) and direct torque control (DTC) [19, 20]. The FOC method realizes the decoupling control of motor torque and flux linkage by controlling the AC and DC components of the stator current respectively. It has the advantages of high steady-state accuracy, good control performance at medium and low speeds. However, in the digital implementation process, the output of the controller lags behind the change of the system current, which affects the static and dynamic response of the current. The DTC method uses a nonlinear hysteresis controller to select an appropriate switching state based on a look-up table logic to achieve independent control of motor torque and flux linkage. It has the characteristics of simple control method, fast dynamic response and strong robustness. DTC methods are generally characterized by strong current and torque ripple, especially at low-speed operation.

In recent years, FCS-MPC has been proposed as an optimal control method in power converters and drivers [21, 22, 23]. The control method predicts system performance based on dynamic models and is implemented by receding horizon optimization. FCS-MPC has the characteristics of fast dynamic response, good current control performance, easy consideration of system nonlinear constraints, and flexible control [24]. Compared with the FOC current control loop, MPC no longer uses the PI regulator, without parameter tuning, directly generates the converter drive signal through the model predictive control algorithm, eliminating the pulse width modulation (PWM) link, and at the same time, it can also use the cost function to increase other control targets and handle system constraints. The main idea of FCS-MPC is to replace the traditional internal current proportional-integral (PI) control loop with a predictive control algorithm [25]. This method avoids the parameter setting of the internal current loop. It reduces the switching frequency and makes it easier to contain system limitations. As described in [26], FCS-MPC has advantages in terms of total harmonics and dynamic response. FCS-MPC and DTC have some similarities. They all have fast dynamic response and a simple control structure. Furthermore, in both methods, only one switching state is selected as the output during the switching period. It is worth mentioning that the difference from DTC is that FCS-MPC selects the best voltage vector through online optimization and is more accurate and effective in vector selection. In addition, FCS-MPC is relatively easy to achieve lower switching frequency and has better steady state performance. According to [27], under the same hardware conditions, the control effect of FCS-MPC is better than DTC.

The traditional PMSM FCS-MPC can obtain the corresponding voltage vector through the switch combination of the inverter, and different current prediction values can be obtained by combining these voltage vectors. By comparing the errors between the predicted current and the reference values, a cost function is optimized which determines

the optimal voltage vector (or the switching state) for the next moment [28]. The traditional current prediction control can obtain good control effects through one-step current prediction, but the one-step current prediction control method has poor stability after the system enters the steady state, and it needs to traverse all the inverter switch combinations during the execution of the algorithm, the amount of online calculation is large. Multi-step prediction can bring good control effects, but it is followed by an exponentially increasing amount of calculation, which is not conducive to online execution [29, 30].

In our work, a three-phase two-level voltage source inverter is considered, which has eight different switching states, including six non-zero switching states and two zero switching states. Usually the two zero switch states are regarded as the same, and thus there are seven switch states in total. The traditional FCS-MPC based on the traversal method needs to predict the current values for seven switch states, from which the optimal one is determined and then sent to the inverter. For a practical motor control system, time-consuming algorithms caused by heavy computations may cause delays during the implementation. The computational burden of the traditional multi-step predictive control algorithms surges as prediction length increases.

This paper uses the method of sector division to reduce the computational complexity in multi-step prediction. First, the cost function is set, and the cost function in the rolling time domain is obtained. The cost function under multi-step prediction is transformed into a least squares problem by matrix transformation. The least squares method can be used to obtain the optimal solution in the ideal state, and the sector in which the composite vector is located can be judged. Finally, it is only necessary to traverse the two switch vectors which constitute the sector and the zero vectors, and select a state vector that optimizes the cost function, which is the switching state adopted at the next moment. The calculation amount of sector division method does not increase exponentially with the increase of the number of prediction steps, only related to the matrix dimension.

Abbreviations. The following abbreviations are used in this manuscript:

PMSM	permanent magnet synchronous motor
FOC	field oriented control
DTC	direct torque control
PWM	pulse width modulation
MPC	model predictive control
CCS-MPC	continuous control set model predictive control
FCS-MPC	finite control set model predictive control
PID	proportional-integral-derivative
ω_e	electrical angle speed
Δt	the sampling interval of discrete system
L, ψ	inductance and flux linkage
i^*	current reference value for comparison with current predicted value
i^p	current predicted value obtained by predictive model
$U(a, b, c)$	the status of the three-phase two-level switch
N	prediction step size
J	state equation of cost function

2. PMSM MPC Strategy.

2.1. Mathematical model of PMSMs. At present, most PMSM control algorithms mainly focus on the following performance indices: the speed error, the harmonic content in the current, the pulsation of electromagnetic torque, and the speed fluctuation when the

load is suddenly added. To achieve the above goals for a PMSM, current loop control is mainly considered. The existing control methods include traditional proportional-integral control, current hysteresis control, neural network control, and sliding mode control, etc. [31, 32]. We mainly consider model-based predictive current control, which takes account of the system dynamics in the control action design. To present the method, the mathematical model of a PMSM is introduced first.

Consider a surface-mounted PMSM, whose model can be expressed as the following [33]

$$\begin{cases} u_d = Ri_d + \frac{d}{dt}\psi_d - \omega_e\psi_q \\ u_q = Ri_q + \frac{d}{dt}\psi_q + \omega_e\psi_d, \end{cases} \quad (1)$$

where u_d and u_q are the stator voltages in d - q frame, i_d and i_q are the stator currents in d - q frame, ω_e is the electrical angle speed, R is the stator resistance, $\psi_d = L_d i_d + \psi_f$ and $\psi_q = L_q i_q$ are the d and q components of the magnetic flux vector, respectively, and ψ_f is the permanent magnet flux linkage. We assume that $L_d = L_q = L$. The stator current can be represented in the following state space model,

$$\begin{bmatrix} \frac{d}{dt}i_d \\ \frac{d}{dt}i_q \end{bmatrix} = \begin{bmatrix} -\frac{R}{L_d} & \omega_e \\ -\omega_e & -\frac{R}{L} \end{bmatrix} \begin{bmatrix} i_d \\ i_q \end{bmatrix} + \begin{bmatrix} \frac{1}{L} & 0 \\ 0 & \frac{1}{L} \end{bmatrix} \begin{bmatrix} u_d \\ u_q \end{bmatrix} - \begin{bmatrix} 0 \\ \frac{\omega_e\psi_f}{L} \end{bmatrix}. \quad (2)$$

According to the Euler formula, one has [34, 35]

$$\begin{cases} \frac{di_d(t)}{dt} \approx \frac{i_d(k+1) - i_d(k)}{\Delta t} \\ \frac{di_q(t)}{dt} \approx \frac{i_q(k+1) - i_q(k)}{\Delta t}. \end{cases} \quad (3)$$

Thus, it holds

$$\begin{bmatrix} i_d(k+1) \\ i_q(k+1) \end{bmatrix} = A(k) \begin{bmatrix} i_d(k) \\ i_q(k) \end{bmatrix} + B \begin{bmatrix} u_d(k) \\ u_q(k) \end{bmatrix} + F(k), \quad (4)$$

where

$$A(k) = \begin{bmatrix} 1 - \frac{\Delta t R}{L} & \Delta t \omega_e(k) \\ -\Delta t \omega_e(k) & 1 - \frac{\Delta t R}{L} \end{bmatrix}, \quad (5)$$

$$B = \begin{bmatrix} \frac{\Delta t}{L} & 0 \\ 0 & \frac{\Delta t}{L} \end{bmatrix}, \quad (6)$$

$$F(k) = \begin{bmatrix} 0 \\ -\frac{\Delta t \psi_f}{L} \omega_e(k) \end{bmatrix}. \quad (7)$$

Defining $x_{dq} = [i_d, i_q]^T$ and $U_{dq} = [u_d, u_q]^T$, Equation (4) can be represented by

$$x_{dq}(k+1) = A(k)x_{dq}(k) + BU_{dq}(k) + F(k). \quad (8)$$

Note that in the above equation the system matrices A and F are dependent on the electrical angle speed ω_e .

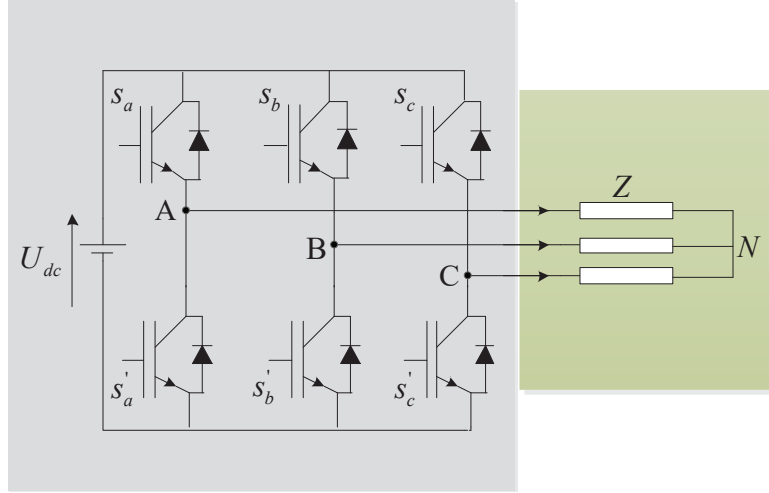


FIGURE 2. The schematic of a three-phase two-level inverter

TABLE 1. The relationship between the switch states and the voltage

Switch state	V_{AN}	V_{BN}	V_{CN}	S_a	S_b	S_c
U_0	0	0	0	0	0	0
U_1	$2U_{dc}/3$	$-U_{dc}/3$	$-U_{dc}/3$	1	0	0
U_2	$-U_{dc}/3$	$2U_{dc}/3$	$-U_{dc}/3$	0	1	0
U_3	$U_{dc}/3$	$U_{dc}/3$	$-2U_{dc}/3$	1	1	0
U_4	$-U_{dc}/3$	$-U_{dc}/3$	$2U_{dc}/3$	0	0	1
U_5	$U_{dc}/3$	$-2U_{dc}/3$	$U_{dc}/3$	1	0	1
U_6	$-2U_{dc}/3$	$U_{dc}/3$	$U_{dc}/3$	0	1	1
U_7	0	0	0	1	1	1

the predicted and the reference current, in such a way that the optimal voltage vector corresponding to the least cost function [36] can be determined.

Eight combinations of switches can yield eight current predictions, with two zero vectors resulting in the same current prediction [37]. Therefore, by comparing the 7 different current prediction values with the current reference value and the limitation of the relevant constraints, the output switching state at the next moment can be obtained.

Consider the surface mount PMSM with $i_d = 0$ control. Therefore, select the reference signal $i_d^* = 0$, i_q^* can be obtained from the PI controller of the speed control loop. For current loop control, the goal of optimization is to minimize the difference between the actual current and the reference current [38] and set the constraint of the magnitude of the stator current. For the above considerations, the cost function corresponding to the current loop is selected as follows

$$\begin{cases} g(k) = \Delta i_d^2 + \Delta i_q^2 + f(k) + \lambda \Delta v(k)^2 \\ \Delta i_d^2 = [i_d^*(k+1|k) - i_d^p(k+1|k)]^2 \\ \Delta i_q^2 = [i_q^*(k+1|k) - i_q^p(k+1|k)]^2, \end{cases} \quad (11)$$

where $\Delta v(k)$ is the switching loss, λ the weighting factor, and the constraint f is only active when the predicted current exceeds its limit value, i.e.,

$$f(k) = \begin{cases} \infty & |i_d^p(k+1|k)| > i_{d\max} \text{ or } |i_q^p(k+1|k)| > i_{q\max} \\ 0 & |i_d^p(k+1|k)| \leq i_{d\max} \text{ and } |i_q^p(k+1|k)| \leq i_{q\max}, \end{cases} \quad (12)$$

where $i_{d\max}$, $i_{q\max}$ are the limits of the d -axis current, and q -axis current, respectively. The three-phase two-level inverter can generate eight combined basic space voltage vectors. As shown in Figure 3, these eight voltage vectors divide the entire plane into six sectors.

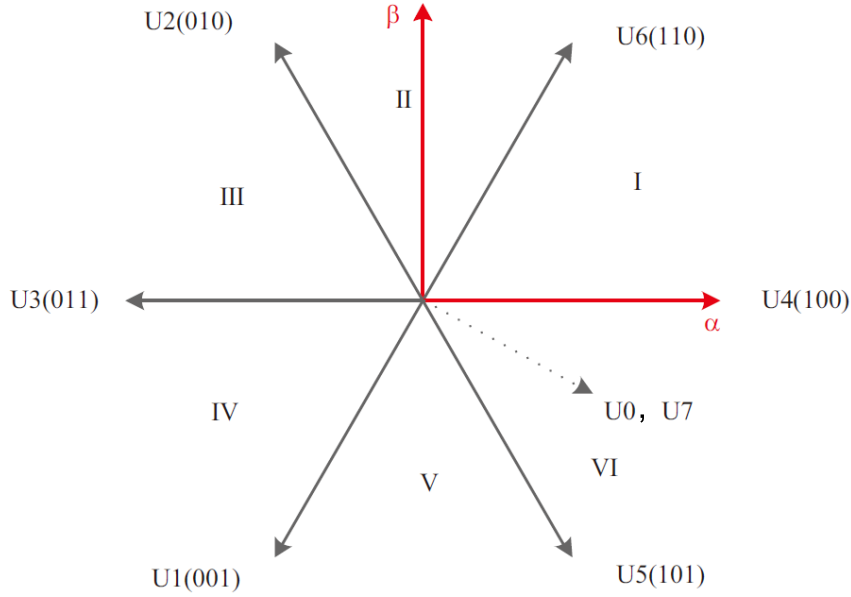


FIGURE 3. Sectorization of space voltage vector

According to Equation (2), one can get u_d^* , u_q^* .

$$\begin{cases} u_d^* = Ri_d + L_d \frac{d}{dt} i_d - \omega_e L_q i_q \\ u_q^* = Ri_q + L_q \frac{d}{dt} i_q + \omega_e (L_d i_d + \psi_f). \end{cases} \quad (13)$$

After transformation, the reference values of u_α^* , u_β^* in the stationary coordinate are obtained. The sector where the desired voltage vector is considered to remain unchanged during a sampling period. The voltage space vector is determined by the switch states. The sectors in which the reference voltage vector is located at the next moment can be judged by u_α^* , u_β^* and Theorem 3.1 which will be presented in the next chapter. Knowing the sector in which the reference voltage vector is located, it is only necessary to traverse the state of the switches that make up the sector.

When using an exhaustive search, the difficulties associated with minimizing g become apparent. In this way, there is no need to traverse all of the switching sequences, simply traverse the switch states that make up the sector and the cost function is evaluated for each such sequence. The switching sequence with the lowest cost is the optimal switching sequence and is selected as the control input. At each step k , searches require the following process [11]:

- 1) For each switching sequence, calculate the state trajectory and the current error according to (11), and consider the current limiting value according to (12);
- 2) Calculate the cost g for the switch states that make up the sector;
- 3) Select the switching order $U_{opt}(k)$ which minimizes the cost function and apply it to the converter.

Repeat the above steps in the next step $k + 1$. The algorithm flow of single step FCS-MPC is shown in Figure 4.

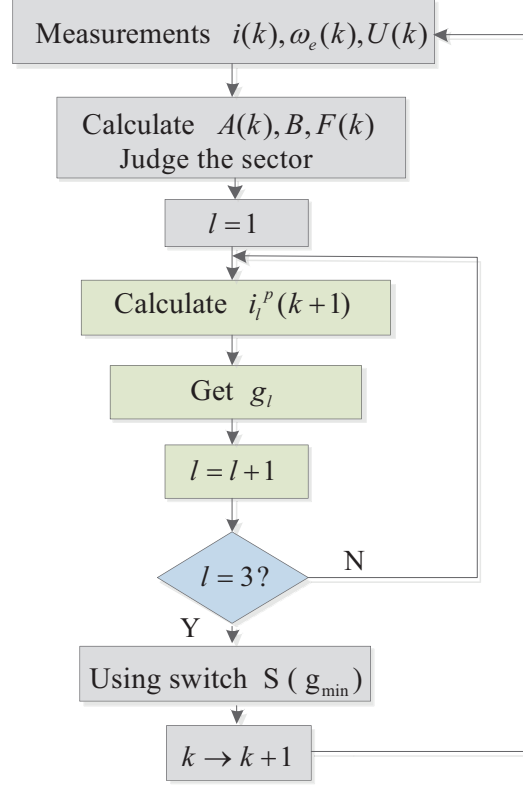


FIGURE 4. The flow chart of single step FCS-MPC

3. Multi-Step FCS-MPC. The principle of multi-step prediction execution is similar to that of single-step prediction, but the computational burden is exponentially increased. Assuming that the rotor speed is constant within the prediction horizon, the vector form of the predicted value of the stator AC and DC currents in the rolling time domain can be obtained [39, 40],

$$x_{dq}(k+i|k) = A^i(k)x_{dq}(k) + [A^{i-1}(k)B\Lambda(k) \dots A^0(k)B\Lambda(k)] U'(k+i-1|k) + [A^{i-1}(k)F(k) + \dots + A^0(k)F(k)], \quad (14)$$

where $i = 1, \dots, N$ with N the prediction horizon length,

$$\Lambda(k) = \frac{2}{3} \cdot \begin{pmatrix} \cos(\omega_e(k)) & \sin(\omega_e(k)) \\ -\sin(\omega_e(k)) & \cos(\omega_e(k)) \end{pmatrix} \cdot \begin{pmatrix} 1 & -\frac{1}{2} & -\frac{1}{2} \\ 0 & \frac{\sqrt{3}}{2} & -\frac{\sqrt{3}}{2} \end{pmatrix}, \quad (15)$$

and

$$U'(k+i-1|k) = [U_{dq}^T(k|k), U_{dq}^T(k+1|k), \dots, U_{dq}^T(k+i-1|k)]^T. \quad (16)$$

Note that although A and Λ are time-varying, i.e., dependent on the motor speed, the matrices A and Λ corresponding to the sampling time instant k are employed during the prediction. The reason lies in the fact that the speed control loop has much slower dynamics compared with the current control loop. Besides, constant system matrices suit for online prediction since the horizon length N is usually not large, and the prediction model results in a neat form. In the rest of this paper, $\cdot(k)$ and A are used instead of $\cdot(k|k)$ and $A(k)$ for simplicity. The prediction model can thus be represented as

$$Y_{dq}(k) = \Gamma x_{dq}(k) + \Upsilon U'(k+N-1|k) + \Pi, \quad (17)$$

where $Y_{dq}(k) = [x_{dq}^T(k+1|k), \dots, x_{dq}^T(k+N|k)]^T$,

$$\Gamma = [A, A^2, \dots, A^N]^T, \quad (18)$$

$$\Upsilon = \begin{bmatrix} B\Lambda & 0 & \dots & 0 \\ AB\Lambda & B\Lambda & \dots & 0 \\ \vdots & \vdots & \vdots & \vdots \\ A^{N-1}B\Lambda & A^{N-2}B\Lambda & \dots & B\Lambda \end{bmatrix}, \quad (19)$$

and

$$\Pi = \left[F, AF + F, \dots, \sum_{j=0}^{N-1} A^j F \right]^T. \quad (20)$$

Now the cost function for the multi-step prediction can be written as

$$J(k) = \|\Gamma x_{dq}(k) + \Upsilon U(k) + \Pi - Y_{dq}^*(k)\|_2^2 + \lambda \|SU(k) - Ev(k-1)\|_2^2, \quad (21)$$

where $Y_{dq}^*(k)$ represents the reference signal for $Y_{dq}(k)$, and it holds

$$S = \begin{bmatrix} I & 0 & \dots & 0 \\ -I & I & \dots & 0 \\ 0 & -I & \dots & 0 \\ \vdots & \vdots & \vdots & \vdots \\ 0 & 0 & \dots & I \end{bmatrix}, \quad E = \begin{bmatrix} I \\ 0 \\ 0 \\ \vdots \\ 0 \end{bmatrix}. \quad (22)$$

By defining

$$\xi(k) = \|\Gamma x_{dq}(k) - \Omega(k)\|_2^2 + \lambda \|Ev(k-1)\|_2^2, \quad (23)$$

$$\Xi(k) = ((\Gamma x_{dq}(k) - \Omega(k))^T \Upsilon - \lambda (Ev(k-1))^T S)^T, \quad (24)$$

and

$$Q = \Upsilon^T \Upsilon + \lambda S^T S, \quad (25)$$

the cost function is equivalent to

$$J(k) = \xi(k) + 2(\Xi(k))^T U(k) + U(k)^T Q U(k), \quad (26)$$

which can be represented as the least squares form

$$J(k) = (U(k) + Q^{-1}\Xi(k))^T Q (U(k) + Q^{-1}\Xi(k)) + c(k), \quad (27)$$

where $c(k)$ is constant within the prediction horizon of the time instant k . Noting that Q is a positive definite matrix, there is a reversible lower triangular matrix H satisfying [41]

$$H^T H = Q. \quad (28)$$

Letting $U_{unc}(k) = -HQ^{-1}\Xi(k)$, the determination of the switch states can be transformed into the following least squares problem

$$U_{opt}(k) = \arg \min_{U(k)} \|HU(k) - U_{unc}(k)\|_2^2. \quad (29)$$

The ideal solution can be defined as $M = -Q^{-1}\Xi(k)$, which is a column vector with $3N$ rows. Correspondingly, $U_0(k) = [M(1), M(2), M(3)]^T$ is the solution for the current time instant k . Note that the vector $U_0(k)$ is the combination of three base vectors, specifically,

$$U_0(k) = M(1)[1, 0, 0]^T + M(2)[0, 1, 0]^T + M(3)[0, 0, 1]^T. \quad (30)$$

It should be noted that $U_0(k)$ is not Boolean in general. Thus it cannot be deployed directly for the switches.

In our proposed approach, the multi-step prediction is considered in order to estimate which sector the optimal solution locates. Afterwards, the sector approach is employed to determine the exact switch states for the time instant k . The sector determination is presented first. To this end, $U_0(k)$ is projected to the α - β axes in the stationary coordinate. The component of $U_0(k)$ corresponding to the α - β axes can be expressed as

$$\begin{cases} u_\alpha = -M(1) + \frac{1}{2}M(2) + \frac{1}{2}M(3) \\ u_\beta = -\frac{\sqrt{3}}{2}M(2) + \frac{\sqrt{3}}{2}M(3). \end{cases} \quad (31)$$

The whole plane is divided into 6 sectors as shown in Figure 5, where the sector numbering is also given. Define P as the sector number associated with the plane division. The determination of the sector number is presented in the following theorem.

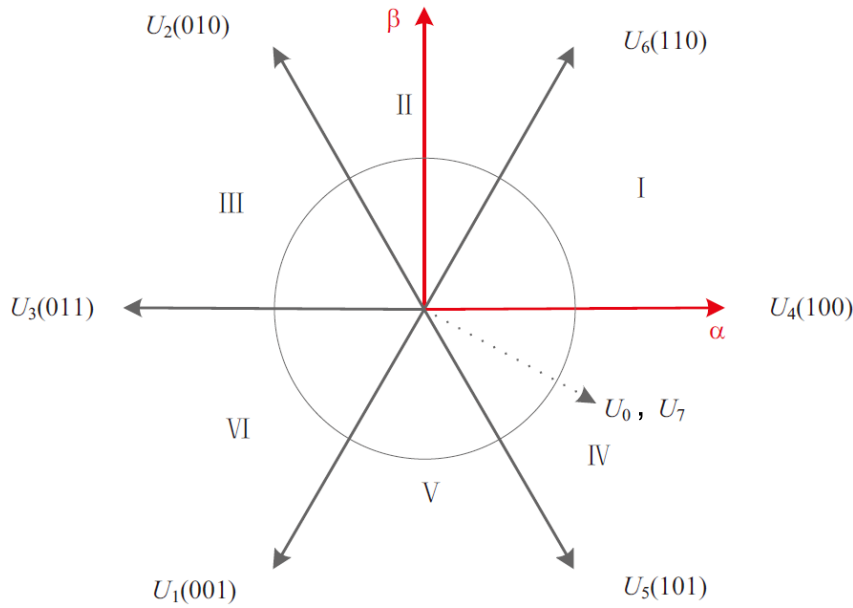


FIGURE 5. Sectorization of space voltage vector

TABLE 2. The relationship between P and the sector numbers

P	1	2	3	4	5	6
Sector	III	II	I	VI	V	IV

Theorem 3.1. Given the normalized vector $[\bar{u}_\alpha, \bar{u}_\beta]^T = [u_\alpha/\sqrt{u_\alpha^2 + u_\beta^2}, u_\beta/\sqrt{u_\alpha^2 + u_\beta^2}]^T$, the sector number P can be determined by $P = \frac{1}{2} \sum_{i=1}^4 (\xi_i + 6)$, where $\xi_1 = \text{sgn}(-\bar{u}_\alpha + 1)$, $\xi_2 = \text{sgn}(-\bar{u}_\alpha + 1/2)$, $\xi_3 = \text{sgn}(-\bar{u}_\alpha - 1/2)$ and $\xi_4 = -3\text{sgn}(\bar{u}_\beta)$.

Proof: We will first discuss the cases that $u_\beta \geq 0$, under which condition 3 sectors are involved, viz. I, II, and III. In order to identify the sector number, we normalize $[u_\alpha, u_\beta]^T$ via $[u_\alpha/\sqrt{u_\alpha^2 + u_\beta^2}, u_\beta/\sqrt{u_\alpha^2 + u_\beta^2}]^T$, and project onto the α -axis. When \bar{u}_α is larger than $1/2$, the sector number $P = 1$. And it holds $P = 3$ if $\bar{u}_\alpha < -0.5$. In others cases, $P = 2$. Based on the above analysis, one has

$$P = \frac{\text{sgn}(-\bar{u}_\alpha + 1) + 1}{2} + \frac{\text{sgn}(-\bar{u}_\alpha + 1/2) + 1}{2} + \frac{\text{sgn}(-\bar{u}_\alpha - 1/2) + 1}{2}, \quad (32)$$

where $\text{sgn}(\cdot)$ is a modified sign function. It holds $\text{sgn}(x) = 1$ if $x \geq 0$ and $\text{sgn}(x) = -1$ if $x < 0$. Above discussion addresses the cases where $\bar{u}_\beta \geq 0$. If $\bar{u}_\beta < 0$, another 3 should be added to the sector number shown in (32). As a result,

$$P = \frac{\text{sgn}(-\bar{u}_\alpha + 1) + 1}{2} + \frac{\text{sgn}(-\bar{u}_\alpha + 1/2) + 1}{2} + \frac{\text{sgn}(-\bar{u}_\alpha - 1/2) + 1}{2} + \frac{-3\text{sign}(\bar{u}_\beta) + 3}{2}. \tag{33}$$

Equation (33) can be simplified as $P = \frac{1}{2} \sum_{i=1}^4 (\xi_i + 6)$ given the definitions of ξ_i , $i = 1, 2, 3, 4$ shown in the theorem. The proof is thus ended. \square

Remark 3.1. *It should be noted that the numbering of the sectors is different from that shown in Figure 3. Such consideration simplifies our analysis in identifying the sector. However, the numbering or sequence is not unique in general.*

After identifying the sector that the ideal solution lies in, the traversing method is employed in order to determine the optimal control input, i.e., the switch states. There are three switch state combinations associated with the selected sector, as shown in Table 3. By comparing the cost function obtained by each switch state combination, the optimal one is determined. Note that the ideal solution M has $3N$ elements, where only the first three elements denote the switch state to be optimized for the current time instant. In the proposed approach, the remainder $3(N - 1)$ elements of M are kept unchanged during the optimization. Specifically the following problem is considered

$$U_{opt}(k) = \arg \min_{U(k) \in \{M_1(P), M_2(P), M_3(P)\}} \|H(U(k) + Q^{-1}\Xi(k))\|_2^2, \tag{34}$$

where $M_i(P)$, $i = 1, 2, 3$ are obtained by replacing the first three elements in M by the three switch states candidates associated with the sector P . The proposed FCS-MPC algorithm is illustrated in Figure 6.

TABLE 3. The switch states corresponding to the sector numbers

P	Switch state that needs to be traversed
1	[0, 0, 0] [0, 1, 0] [0, 1, 1]
2	[0, 0, 0] [0, 1, 0] [1, 1, 0]
3	[0, 0, 0] [1, 0, 0] [1, 1, 0]
4	[0, 0, 0] [1, 0, 0] [1, 0, 1]
5	[0, 0, 0] [0, 0, 1] [1, 0, 1]
6	[0, 0, 0] [0, 1, 1] [0, 0, 1]

Remark 3.2. *In the traditional multi-step FCS-MPC method, 2^{3N} switch states need to be traversed and compared. However, in the proposed method only 3 switch states are traversed. Hence, the computational burden is significantly reduced.*

Remark 3.3. *Compared with traditional control algorithms, such as FOC and DTC, the multi-step model predictive control algorithm proposed in this paper can continuously perform receding-horizon optimizations based on the established PMSM mathematical model, which renders smaller speed error and thus better control performance. In addition, the traditional multi-step prediction algorithm relies on the traversal method, the computational burden increases exponentially as the prediction length increases. Thus it restricts to short prediction horizons in practical applications, e.g., one step prediction is usually considered. Although some approaches have been proposed to alleviate the computational*

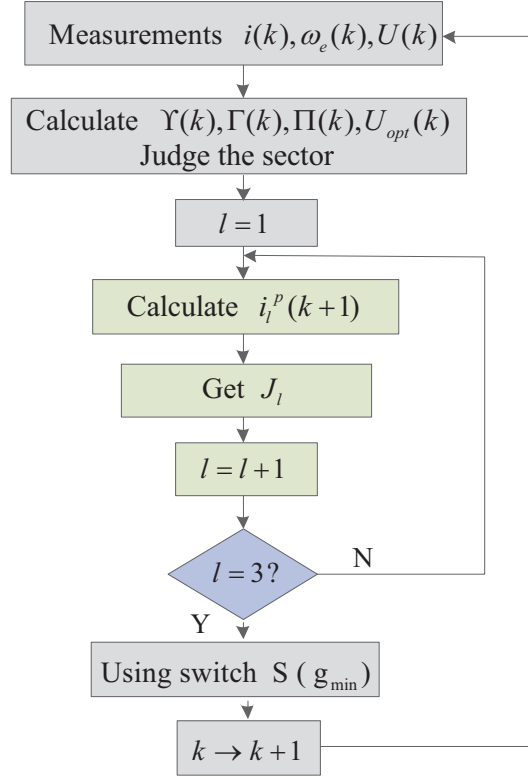


FIGURE 6. The algorithm flow chart of FCS-MPC based on sector division

issue, e.g., the sphere decoder algorithm [40, 41], it is noticed that the relevant algorithms are relatively complicated during the implements. The feature of the propose multi-step prediction approach lies in the fact that it considers both the computational burden and the ease in implementation.

4. Simulation Results. To verify the effectiveness of the proposed control algorithm, we built two sets of simulation model in the MATLAB/Simulink environment. One set of simulations compared FCS-MPC based on sector division method with FCS-MPC based on traversal method, and another set of simulations compared FCS-MPC based on sector division method with the space vector pulse width modulation algorithm based on proportional-integral controller (PI-SVPWM), which is currently the most widely used method in industry. The parameters of the PMSM motor used in the simulations are shown in Table 4.

TABLE 4. The table of motor parameters

Parameters	Symbol	Value	Units
Power rating	P_N	2.2	kW
Rated voltage	U	380	V
Rated current	I	5	A
Rated frequency	f	75	Hz
Rated speed	r	1500	rad/s
Number of pole pairs	p	3	
Stator resistance	R_s	2.75	Ω
d - q component of the stator inductance	L	40	mH
Flux linkage of permanent magnet	Ψ	0.44	Wb

Figure 7 shows the speed and the three-phase current control based on the traversal and sector division method FCS-MPC. The figure shows the speed and current control waveforms for single-step prediction and three-step prediction. It can be seen the speed fluctuation of the three-step prediction after the speed enters the steady state is significantly smaller than the speed fluctuation under the single-step prediction. Also the three-phase current under the three-step prediction has less fluctuation after entering the steady state than the single-step prediction. Figure 8 shows the speed and the q -axis current comparison based on sector division based FCS-MPC and PI-SVPWM. For both cases where $N = 1$ and $N = 3$, the control performance of FCS-MPC based on sector division method is much better than that of PI-SVPWM. When the motor starts, faster speed responses and smaller overshoots are observed. At time $t = 2$ s, the load is suddenly added, it can be shown that the speed change is relatively small and it can quickly follow the reference signal. Therefore, the FCS-MPC control algorithm based on sector division has stronger robustness. PI-SVPWM requires additional pulse width modulation, though its q -axis current pulsation is smaller.

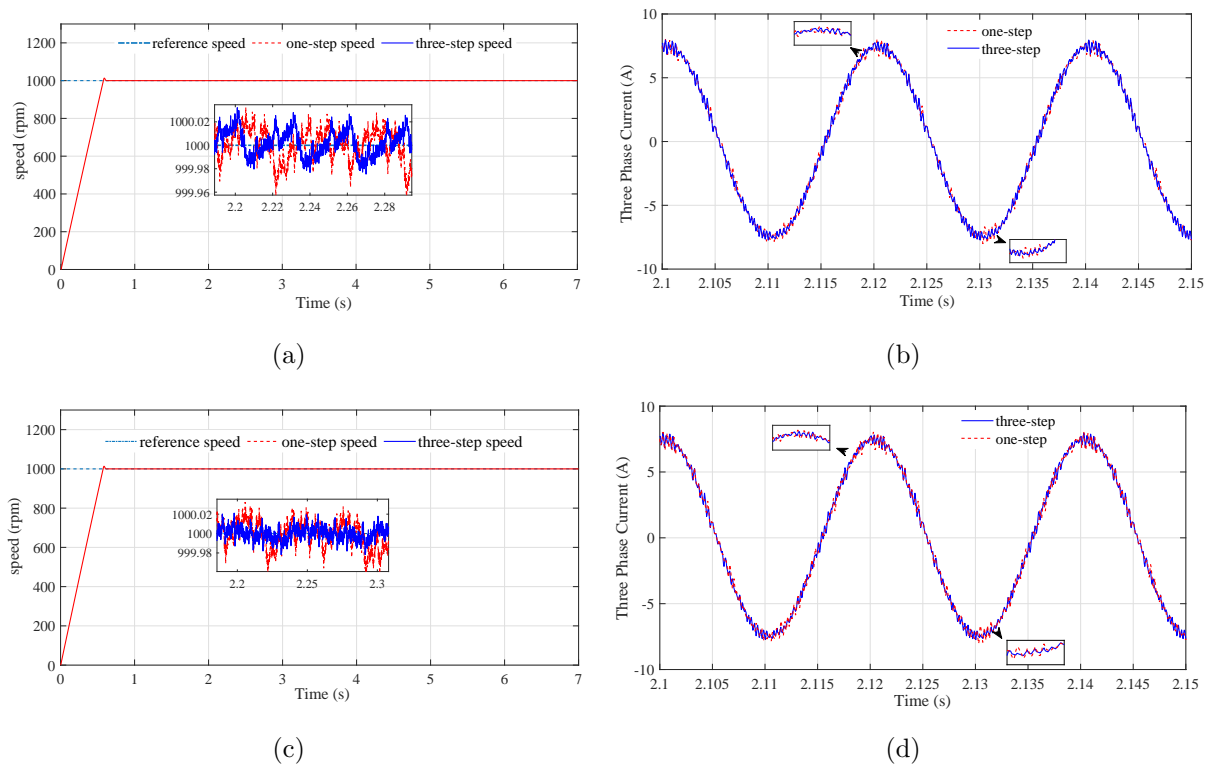


FIGURE 7. Comparison of speed and current at a given speed of 1000 rpm. Figures (a) and (b) show the one-step and three-step speed and three-phase current comparison based on the traversal method. Figures (c) and (d) show the one-step and three-step speed and three-phase current comparison based on the sector division method.

From Figure 7 and Figure 8, it can be found that the sector division method and the traversal method can improve the control effect by increasing the prediction step size. The control effect of the sector partition method in single-step prediction is almost the same as that of the traversal method. Since the calculation amount is not very large in single-step prediction, the algorithm is less affected when the switch state is executed online. By comparing the speed and current waveforms under the three-step prediction, it

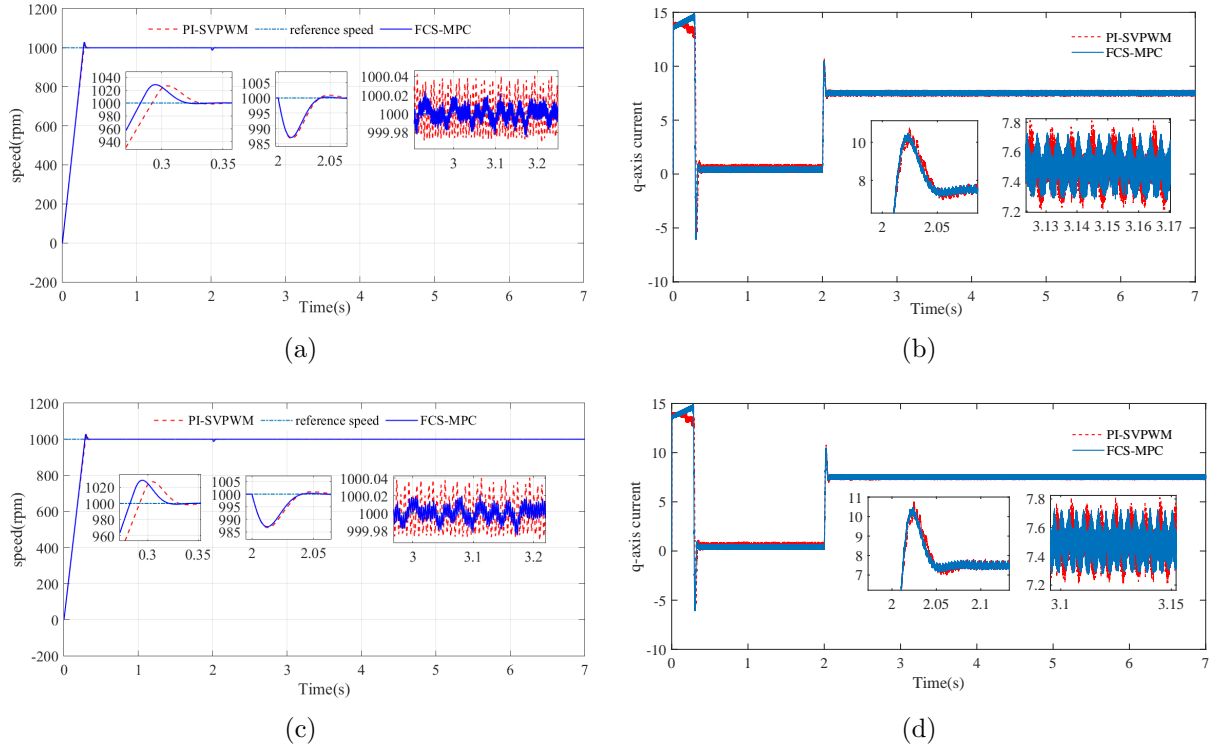


FIGURE 8. Comparison of speed and current at a given speed of 1000 rpm. Figure (a) shows the speed comparison between one-step FCS-MPC with PI-SVPWM. Figure (c) shows the speed comparison between three-step FCS-MPC with PI-SVPWM. Similarly, Figures (b) and (d) show the q -axis current using different methods.

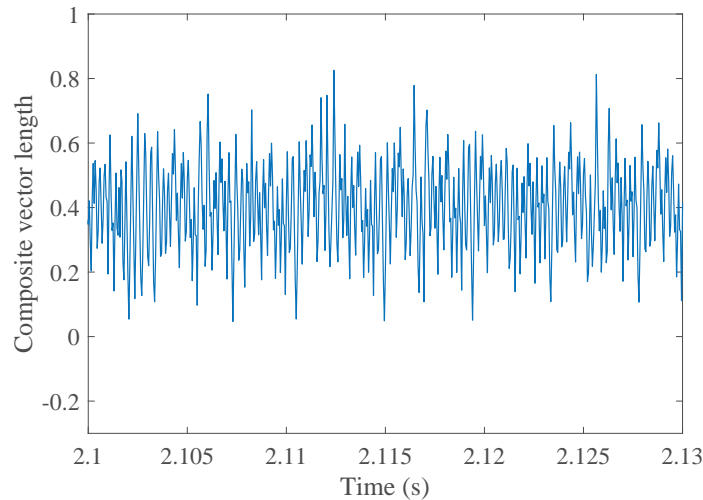


FIGURE 9. Composite vector length in sector division method

can be found that the control effect of the FCS-MPC based on the sector division method is better than the traversal method, and the online execution time required by the sector division method is much smaller than the traversal method, which is conducive to the execution of the system. Figure 9 shows the composite vector length obtained by the sector division method. The length of the composite vector ranges from 0 to 1, which also proves the reliability of the proposed algorithm.

Table 5 compares the time consumed by the traversal method and the sector division method in the multi-step prediction. The amount of calculation required for traversal method increases exponentially with the increase of the prediction steps. The calculation amount of sector division method does not increase exponentially with the increase of the number of prediction steps, only related to the matrix dimension.

TABLE 5. The comparison of computation

Predicted steps	Traversal time required/ μs	Sector division time required/ μs
1	2.2	2.1
3	24.3	4.6
5	603.4	6.4

5. Conclusion. In this paper, a multi-step predictive control method for permanent magnet synchronous motor based on sector division algorithm is proposed. By transforming the cost function into a least squares problem through matrix transformation, the optimal solution of the cost function in the ideal state is obtained, and the three vectors of the optimal solution in the ideal state are synthesized and the sector in which the composite vector is located is determined. Finally, the amount of calculation of multi-step prediction is reduced by the sector division method. The simulation results show the comparison of the time consumed by the traversal method and the sector partitioning method. The results show that the amount of computation required by the sector partitioning method for multi-step prediction does not increase sharply with the increase of the prediction step size, and only a small amount of computation increases while bringing better control effects.

Acknowledgment. This work was partially supported by the National Natural Science Foundation of China (61903158, 61973140), National first-class discipline program of Food Science and Technology (JUFSTR20180205), and the National Science Foundation of Jiangsu Province of China (BK20180595).

REFERENCES

- [1] F. Wang, Z. Zhang, A. Davari et al., An experimental assessment of finite-state predictive torque control for electrical drives by considering different online-optimization methods, *Control Engineering Practice*, vol.31, pp.1-8, 2014.
- [2] X. Liu, M. Liu and Y. Shi, Event triggered model predictive control: A less conservative result, *Journal of the Franklin Institute*, vol.355, no.18, pp.9053-9071, 2018.
- [3] M. Morari and J. H. Lee, Model predictive control: Past, present and future, *ISA Transactions*, vol.33, pp.235-243, 1999.
- [4] T. Shi, P. Shi and S. Wang, Robust sampled-data model predictive control for networked systems with time-varying delay, *International Journal of Robust and Nonlinear Control*, vol.29, no.6, pp.1758-1768, 2019.
- [5] L. Cavanini, G. Cimini and G. Ippoliti, Model predictive control for pre-compensated power converters: Application to current mode control, *Journal of the Franklin Institute*, 2019.
- [6] P. Cortes, M. P. Kazmierkowski, R. M. Kennel et al., Predictive control in power electronics and drives, *IEEE Transactions on Industrial Electronics*, vol.55, no.12, pp.4312-4324, 2008.
- [7] T. Geyer, Computationally efficient model predictive direct torque control, *IEEE Transactions on Power Electronics*, vol.26, no.10, pp.2804-2816, 2011.
- [8] P. Karamanakos, T. Geyer and R. Kennel, Computationally efficient optimization algorithms for model predictive control of linear systems with integer inputs, *2015 the 54th IEEE Conference on Decision and Control (CDC)*, 2015.

- [9] D. E. Quevedo, G. C. Goodwin et al., Moving horizon design of discrete coefficient FIR filters, *IEEE Transactions on Signal Processing*, vol.53, no.6, pp.2262-2267, 2005.
- [10] J. S. Hu and K. Y. Chen, Analysis and design of the receding horizon constrained optimization for class-D amplifier driving signals, *Digital Signal Processing*, vol.20, no.6, pp.1511-1525, 2010.
- [11] S. Vazquez, J. Rodriguez, M. Rivera et al., Model predictive control for power converters and drives: Advances and trends, *IEEE Transactions on Industrial Electronics*, vol.64, no.2, pp.935-947, 2017.
- [12] S. Yang, A. H. Ghasemi, X. Lu et al., Pre-compensation of servo contour errors using a model predictive control framework, *International Journal of Machine Tools & Manufacture*, vol.98, pp.50-60, 2015.
- [13] J. I. Leon, S. Kouro, L. G. Franquelo et al., The essential role and the continuous evolution of modulation techniques for voltage-source inverters in the past, present, and future power electronics, *IEEE Transactions on Industrial Electronics*, vol.63, no.5, pp.2688-2701, 2016.
- [14] T. Laczynski and A. Mertens, Predictive stator current control for medium voltage drives with LC filters, *IEEE Transactions on Power Electronics*, vol.24, pp.2427-2435, 2009.
- [15] T. Geyer, P. Karamanakos and R. Kennel, On the benefit of long-horizon direct model predictive control for drives with LC filters, *Energy Conversion Congress & Exposition*, pp.3520-3527, 2014.
- [16] K.-C. Yao, T.-C. Wu, L.-C. Hsu and W.-T. Huang, Evaluating thematic-approach teaching of robot design and practice course through psychomotor and affective domains, *ICIC Express Letters*, vol.13, no.1, pp.41-49, 2019.
- [17] T. Wang and H. Ma, The research of PMSM RBF neural network PID parameters self-tuning in elevator, *2015 the 27th Chinese Control and Decision Conference (CCDC)*, Qingdao, pp.3350-3354, 2015.
- [18] H. Sun, R. Dong and Y. Zhang, An improved stochastic gradient algorithm to identify PMSM parameters based on CAR models, *2017 the 36th Chinese Control Conference (CCC)*, Dalian, pp.2076-2081, 2017.
- [19] L. M. Corradini, G. Ippoliti and G. Orlando, Fault-tolerant sensorless control of wind turbines achieving efficiency maximization in the presence of electrical faults, *Journal of the Franklin Institute*, vol.355, no.5, pp.2266-2282, 2018.
- [20] M. Marufuzzaman, M. B. I. Reaz, M. S. Rahman et al., Hardware prototyping of an intelligent current dq PI controller for FOC PMSM drive, *International Conference on Computer Applications & Industrial Electronics*, pp.86-88, 2011.
- [21] C. S. Lim, E. Levi, M. Jones et al., FCS-MPC-based current control of a five-phase induction motor and its comparison with PI-PWM control, *IEEE Transactions on Industrial Electronics*, vol.61, no.1, pp.149-163, 2014.
- [22] M. Narimani, B. Wu, V. Yaramasu et al., Finite control-set model predictive control (FCS-MPC) of nested neutral point clamped (NNPC) converter, *IEEE Transactions on Power Electronics*, vol.30, no.12, pp.7262-7269, 2015.
- [23] S. A. Davari, D. A. Khaburi, R. Kennel et al., Using a weighting factor table for FCS-MPC of induction motors with extended prediction horizon, *Conference of the IEEE Industrial Electronics Society*, 2012.
- [24] S. Vazquez, J. I. Leon, L. G. Franquelo et al., Model predictive control: A review of its applications in power electronics, *IEEE Industrial Electronics Magazine*, vol.8, no.1, pp.16-31, 2014.
- [25] M. Trablesi, S. Bayhan, H. Abu-Rub et al., Finite control set model predictive control for grid-tie quasi-Z-source based multilevel inverter, *IEEE International Conference on Industrial Technology (ICIT)*, pp.299-304, 2016.
- [26] M. P. Kazmierkowski, High performance control of AC drives with MATLAB/Simulink models, *IEEE Industrial Electronics Magazine*, vol.6, pp.68-69, 2012.
- [27] F. Morel, X. Lin-Shi, J. M. Retif et al., A comparative study of predictive current control schemes for a permanent-magnet synchronous machine drive, *IEEE Transactions on Industrial Electronics*, vol.56, no.7, pp.2715-2728, 2009.
- [28] J. Rodríguez, R. M. Kennel, Espinoza, R. José et al., High-performance control strategies for electrical drives: An experimental assessment, *IEEE Transactions on Industrial Electronics*, vol.59, no.2, pp.812-820, 2012.
- [29] P. Karamanakos, T. Geyer, R. Kennel et al., Reformulation of the long-horizon direct model predictive control problem to reduce the computational effort, *IEEE Energy Conversion Congress and Exposition (ECCE)*, pp.3512-3519, 2014.

- [30] D. Zhang, P. Shi, W. A. Zhang et al., Energy-efficient distributed filtering in sensor networks: A unified switched system approach, *IEEE Transactions on Cybernetics*, vol.47, no.7, pp.1618-1629, 2017.
- [31] E. Lu et al., Anti-disturbance speed control of low-speed high-torque PMSM based on second-order non-singular terminal sliding mode load observer, *ISA Transactions*, vol.88, pp.142-152, 2019.
- [32] J. Yu, P. Shi, W. Dong, B. Chen and C. Lin, Neural network-based adaptive dynamic surface control for permanent magnet synchronous motors, *IEEE Transactions on Neural Networks and Learning Systems*, vol.26, no.3, pp.640-645, 2015.
- [33] S. L. Kellner, B. Piepenbreier et al., General PMSM d,q-model using optimized interpolated absolute and differential inductance surfaces, *IEEE International Electric Machines & Drives Conference (IEMDC)*, pp.212-217, 2011.
- [34] Z. Zhang, J. Schenek, R. Kennel et al., Direct model predictive control of five-level dual flying capacitor active neutral point clamped converters with modified sphere decoding, *Transportation Electrification Conference & Expo*, vol.32, pp.350-355, 2017.
- [35] M. Habibullah, D. C. Lu, D. Xiao et al., Finite-state predictive torque control of induction motor supplied from a three-level NPC voltage source inverter, *IEEE Transactions on Power Electronics*, vol.32, no.1, pp.479-489, 2017.
- [36] L. Wang, S. Chai, D. Yoo et al., *PID and Predictive Control of Electrical Drives and Power Converters Using MATLAB/Simulink*, Wiley-IEEE Press, 2015.
- [37] G. Q. Chen and J. L. Kang, Spectrum analysis methods to the two-level three-phase inverter, *Key Engineering Materials*, vols.467-469, pp.968-971, 2011.
- [38] L. Cavanini, G. Cimini, G. Ippoliti et al., Model predictive control for pre-compensated voltage mode controlled DC-DC converters, *IET Control Theory & Applications*, vol.11, no.15, pp.2514-2520, 2017.
- [39] T. Geyer and D. E. Quevedo, Multistep finite control set model predictive control for power electronics, *IEEE Transactions on Power Electronics*, vol.29, no.12, pp.6836-6846, 2014.
- [40] P. Karamanakos, T. Geyer, T. Mouton et al., Computationally efficient sphere decoding for long-horizon direct model predictive control, *Energy Conversion Congress & Exposition*, pp.1-8, 2016.
- [41] T. Geyer and D. E. Quevedo, Multistep direct model predictive control for power electronics – Part 2: Analysis, *Energy Conversion Congress & Exposition*, pp.1162-1169, 2013.